Science & Technology Facilities Council

Technical Report
RAL-TR-2012-002

The OSMOND detector

JE Bateman, R Dalgliesh, DM Duxbury, WI Helsby,
SA Holt, D McPhail, AS Marsh, NJ Rhodes,
EM Schooneveld, EJ Spill, R Stephenson

February 2012

RAL Library
STFC Rutherford Appleton Laboratory
R61
Harwell Oxford
Didcot
OX11 0QX

Tel: +44(0)1235 445384
Fax: +44(0)1235 446403
email: libraryral@stfc.ac.uk

Science and Technology Facilities Council reports are available online at: http://epubs.stfc.ac.uk

ISSN 1358- 6254

THE OSMOND DETECTOR

J.E.Bateman, R. Dalgliesh, D.M.Duxbury, W.I.Helsby, S.A.Holt, D. M^{c}Phail, A.S.Marsh, N.J.Rhodes, E.M.Schooneveld, E.J.Spill and R.Stephenson

Science and Technology Facilities Council, Rutherford Appleton Laboratory, Harwell Science and Innovation Campus, Didcot, Oxfordshire, OX11 0QX, U.K.

31st January 2012

Abstract

The development and testing of the Off Specular MicrOstrip Neutron Detector (OSMOND) is described. Based on a Microstrip Gas Chamber the aim of the project was to produce a high counting rate detector capable of replacing the existing rate limited scintillator detectors currently in use on the CRISP reflectometer for off specular reflectometry experiments. The detector system is described together with results of neutron beam tests carried out at the ISIS spallation neutron source.

1. Introduction

Since the Gas Microstrip detector (MSGC) was introduced over 20 years ago at the ILL [1], several institutions have used it as the basis for a whole suite of neutron detector applications. In our own development program we have shown that these devices offer great potential to replace existing ^{3}He tube neutron detectors and can be successfully operated as 2D imaging detectors [2,3].

The CRISP reflectometer [4,5] is an instrument which is primarily used for time of flight neutron reflection experiments from surfaces and interfaces. The instrument is used to look at either specular or off specular reflection from the sample with both modes utilising separate detection systems. For specular reflection, the intensity of the reflected beam is measured with a single element detector but for off specular reflection a multi element position sensitive detector is needed. This is currently done with a linear position sensitive fibre coded ZnS:Ag/^{6}LiF scintillation detector. This scintillation detector is limited to a position resolution of 1.2mm and is limited in count rate performance at the highest rates delivered from CRISP.

Operation of MSGC based detectors has been demonstrated at count rates of up to 1MHz/mm^2 of plate [6] with useful counter lifetimes corresponding to months of continuous running at these rates [7]. In order to make the detector neutron sensitive ^{3}He is used owing to its large cross section for 1Å neutrons (3000 barns) and the reaction mechanism is highlighted below:

$$ {}^{3}_{2}He + {}^{1}_{0}n \rightarrow {}^{1}_{1}H + {}^{3}_{1}H + 764keV $$

This technology can offer a high rate capability detector with good timing resolution and low gamma sensitivity at high neutron detection efficiencies in the 1-10Å wavelength range. The inevitable trade off between neutron detection efficiency and spatial resolution is set by the counter depth, the gas pressure and the electronic discriminator threshold. This trade off is largely determined by the range of the reaction products from the ^{3}He-neutron reaction (a proton and a triton) which can conveniently be examined by the use of a Monte Carlo model of the interaction of these particles with the gas mixture. Such a study was previously undertaken [8] focusing on the following performance criteria:

- a position resolution of 0.5mm or better (FWHM)
- a neutron detection efficiency $\geq$ 50% @ 1Å
- a local count rate performance of at least 10^5 counts per second per channel
- a counting dynamic range of 6 orders of magnitude

The conclusion of the study was that it should be possible to build a detector to satisfy these criteria, based on an MSGC in which the anode strips are made to point at the sample position, whilst the neutron induced electron clouds are drifted perpendicularly to the direction of the neutron beam. This ‘pointing anode’ geometry also gives parallax free detection in an almost identical fashion to the HOTWAXS detector [9]. A programme of work was then undertaken to produce such a detector, called

OSMOND (Off Specular MicrOstrip Neutron Detector), and this report will describe the detector design, performance characteristics and the results of the neutron beam tests performed on the CRISP reflectometer.

2. Detector Design

The OSMOND detector consists of 5 gas microstrip detector modules located on a precision mounting plate which can be seen in figure 1. Each module subtends 1.9^{o} with an electrode design that points to a sample position some 1.87m away giving a complete angular range of 9.5^{o}. This mounting plate is bolted to a bulkhead plate, which together with the detector body forms the gas envelope. A gas inlet pipe is welded into the vessel and is sealed off with a Swagelok valve [10]. The vessel is rated to a working pressure of 14 bars and the gas seal is made by using a Garlock metal seal [11].

A drift plane placed 50mm above the detector modules, within the gas volume, defines the active aperture of the detector. Neutrons enter the gas volume through the vessel body, parallel to the plate surface, where they interact with the gas. The electrons formed in the gas then drift down to the plate surface where avalanche multiplication takes place and induces a pulse on the MSGC anodes. The section of the vessel body, through which the neutrons enter, has been thinned in order to reduce the neutron scattering and absorption in the window. Behind the entrance window and before the active region of the MSGC plates, is a 'dead region' of gas. This is filled with a displacing material so that a minimum number of neutrons are absorbed before the active region of the detector. This 'displacer' has been made from a single piece of curved amorphous quartz, 11mm thick and ~350mm long, on a radius of curvature of 1.87m. Previous measurements on ISIS [12] show that the transmission of 10mm of quartz is of the order of 0.83 over our working wavelength range of 1-5Å.

2.1 The MSGC module

The OSMOND MSGC's are of the 'pointing anode' design described previously [9], thus offering a parallax free geometry. Each glass plate consists of 128 anodes of 10μm width and 65mm in active length. These are interleaved with cathodes of varying width on a pitch of 483μm at a radius of 1.87m, to 500μm at a radius of 1.935m and are produced in a chrome process at IMT [13] on Schott S8900 semi-insulating glass [14]. They are designed such that two plates can be mounted beside each other with no dead region in the angular coverage, achieved by utilising a 'half cathode' on both edges of the plate and by the precision mounting of the modules. The plates themselves are glued to a ceramic printed circuit board (PCB) which offers mechanical support and are ultrasonically wire bonded to pads on the PCB which are tracked to two JAE 70 pin connectors [15]. The PCB is then glued, using Torrseal [16] to a precision mounting block while being accurately located in an assembly jig. The signals from the two connectors on the ceramic board are then fed, via kapton flexi-rigids, to a Martech (or Allectra) [17] 144 way feed-through flange, out of the gas volume to charge sensitive preamplifiers housed behind the curved bulkhead plate. The feed-through flanges are

pressure rated to 21 bars and have been custom built to our specification. Signals from the 640 independent channels are then passed to a bank of amplifier-discriminators housed in a remote VME rack, via 25m long cables, where the signals are processed further. The amplifier-discriminator boards can be programmed to gain normalise the signals and to adjust the DC offsets of all channels independently. The discriminators are then interrogated by a ripple priority encoder (RPE) which determines the neutron event position and then passes this information to the ISIS data acquisition electronics (DAE) system [18].

As mentioned above, the plate is designed to point at the sample position but this non-uniform electrode structure can introduce non-uniformities in the gain of the MSGC along the strip length. Previous work has shown that this non-uniformity can be minimised by carefully grading the anode-cathode gap width with the pitch of the tracks [19] and by using the empirically determined formula given in [20]. The plates have been designed accordingly and because the tapering on the plates is not too severe (cathode width varies by 7μm over the active length) the gain variation from the front to the back of the strips is within 10%.

2.2 Detector modularity

The modularity of the OSMOND detector gives the flexibility of individually testing each MSGC module, in an X-ray sensitive atmosphere, before installation within the pressure vessel housing. A test box utilising a flowing gas system, previously constructed for the HOTWAXS module measurements, was used for this purpose as it included the necessary multi-way feed-through connector. A standard Ortec preamp/post amplifier combination was used to measure the gas gain of the MSGC plate using the signals from an ^{55}Fe X-ray source and a typical pulse height spectrum obtained from the sum of 4 neighbouring channels is shown in figure 2. An energy resolution of 15.4% FWHM was obtained which compares favourably with the 14.3% obtained from the HOTWAXS geometry [9]. Figure 3 shows gain curves from the OSMOND module compared to a HOTWAXS module in an argon:isobutane 75:25 gas mixture. The gain uniformity over a complete module was measured taking a pulse height spectrum over groups of four neighbouring channels. Figure 4 shows the variation of the gain and sigma (the fractional standard deviation) of the pulse height distribution across a full module. As can be seen in the figure, the majority of the data obtained is very uniform but both ends of the module give anomalous results due to the discontinuity in the drift field in the test box. In the fully assembled detector, each module butts up to a neighbouring module, maintaining a uniform drift field, except at the two outer ends of the whole detector where the edge field correctors negate this effect. If we ignore the end points, the residual variation in gain is 1.8% and the variation in sigma is 1.3%, confirming that the gas gain is very uniform over the whole plate area. The weak sixteen channel periodicity in the gain arises from the grouping of the tracks between the plate and the bulkhead connector.

Figure 5 shows the uniformity of response achieved over the whole detector using the flood beam generated by the irradiation of a thick polyethylene sample by the neutron beam on CRISP. This gives an approximately uniform flood which is smooth and can be

fitted well with a simple second order polynomial (indicated in the figure) to show up the local variations in the detector response. The lower curve shows a single exposure of 180μA-hr of beam and the upper curve shows the sum of seven such runs with the dozen or so obviously faulty channels interpolated. The fit yields a standard error (sigma) of 8% which is clearly due to a fair number of aberrant channels. When the fitting range is confined to a clean region (e.g. channel 75 to 125) a sigma of 2.1% is obtained including a statistical contribution of 1.5%. This level of uniformity is that to be expected from the intrinsic limit set by electronic component tolerances but clearly work is required to identify and correct the many channels which show obvious problems, which will be carried out in due course. In the application to reflectometry, as will be shown below, the presence of the "rogue" channels does not interfere seriously with the usefulness of the detector.

2.3 Digital readout system

A custom designed readout was developed in house to interface the 640 independent readouts of the detector to a single ISIS DAE channel. This inevitably seriously restricts the global acquisition rate limit of the detector but is essential to access the current ISIS DAE system. This system (the RPE) operates on the individual channel discriminator outputs and is situated on the backplane on the VME crate which houses them.

Events present in any channel of the detector in which the input pulse is above the discriminator lower level threshold (LLD) start the priority encoding. All the discriminator outputs are sent through a normally transparent latch and are OR'd together to form a raw trigger signal. This signal is delayed for 40 ns to allow any neighbouring discriminator pulses to settle, and then fed back to all the discriminators to hold the discriminator signals latched. If there is a second event within this 40ns, both hits are held and readout, but this will appear as a wide hit and both events will be rejected later. After the 40ns delay the discriminator signal is held latched for 300ns, during which time any other events will be rejected. In the 300ns, the priority encoder settles with "carry" signals rippling from left to right and right to left across the backplane to find the left most and the right most edges of the hit. After the 300ns delay the central controller issues a latch signal which latches the position of the left most and right most sides of the hit or hits and the latch holding the discriminator outputs is released. This takes a further 30ns after which the front end can then begin accepting events again. A read signal is then sent to the discriminator boards and the cards containing the left and right most edges output their position. The left and right most edges are processed in the central controller to determine the position of the event, which is (left + right) / 2 and the width which is 1 + right - left. Events triggering a double hit are arbitrarily assigned to the leftmost channel.

The front-end electronics are a replica of the HOTWAXS system [9] with each strip capable of being counted in its own scaler with a channel deadtime of ~200ns. In one of its test modes the counter can operate in this way yielding a rate capability which the CRISP beam cannot seriously challenge (at the maximum rate used the estimated

deadtime per channel does not exceed a few percent). In the rate tests described below this measurement is referred to as the "raw rate" and is the best estimate of the actual rate incident on the detector.

3. System performance

With the five MSGC modules mounted in the pressure vessel, the performance of the OSMOND detector with a ^{3}He based gas mixture was investigated. A 350GBq moderated ^{241}Am:Be source was used to provide the neutrons for the initial characterisation. The detector was designed to operate with a maximum operating pressure of 14 bars of gas, nominally five bars ^{3}He and five bars CF_4. However, the majority of the results reported in this paper have been obtained with a mixture of 3.6 bars ^{3}He and 4.0 bars of CF_4.

3.1 Basic properties

A typical pulse height spectrum obtained from the sum of four adjacent channels is shown in figure 6, with the standard operating voltages of -1200V across the anode cathode gap and -20kV applied to the drift. A clear peak (FWHM 11.7%) is observed corresponding to the full deposit of the 764keV energy deposit from the detection nuclear reaction. This peak was used to measure the gain curve shown in figure 7. The figure also shows the data obtained when the detector was filled with 0.5 bars ^{3}He and 1.5 bars of CF_4. In both gas mixtures the spark limit was not reached. The gains obtainable are low, by the standards of X-ray detectors, but this is compensated by the fact that the initial charge produced from the ^{3}He (n,α) reaction is $\times$100 greater than the typical X-ray signal. A gas gain of $\times$10 is then sufficient to bring the charge signal into the comfortable working range of 2-3$\times10^5$ electrons. One proviso is that the gain should be high enough to ensure that the temporal pulse formation is kept stable and short, but a gain of $\times$10 seems more than adequate to assure this given the small dimensions of the MSGC section.

At the high pressures required for efficient operation, the drift field must be sufficient to ensure effective charge collection onto the MSGC anodes. Two physical processes affect this. First, the electron clouds spread by diffusion during the drift process with the possibility of degrading the pulse height spectrum. The second effect can be caused by electron attachment during the drift process, leading to highly distorted pulse height spectra and loss of signal. A simple measurement can confirm that neither of these two effects is seriously present. It has been shown elsewhere [21] that the gain of an MSGC with a drift section and perfect charge collection is dependent on the parameter $V_b + \alpha V_d$ (where V_d is the drift voltage and V_b is the bias voltage of the MSGC plate and α is a constant << 1) so that plotting V_b versus V_d at constant gain should give a straight line if no drift loss processes are significant. Figure 8 shows such a plot with a reasonable straight line fit, which together with the excellent pulse height spectra, gives total confidence in the operation of the detector.

The operational stability of OSMOND is important both in the short term, where the detector needs to operate stably over 4-5 days (typical of experimental runs on ISIS) and in the longer term, over a complete ISIS cycle (6 weeks). Initial gain measurements indicated satisfactory stability over a period of 9 days, after which OSMOND was mounted on the CRISP beamline. Due to the exigencies of beam access, continuous monitoring of the detector gain was not practicable. However, it was found that after 236 days of continuous biasing the gain was exactly the same as at the start within the experimental error. No change in the operating voltages was needed over several sessions of beam exposure giving reassurance of adequate stability.

As for possible beam-induced ageing effects, none were seen over a total exposure estimated at about ~360 hours. Confirmation of stability in this context must await the installation of the detector on an instrument for regular use; there is no reason to have any anxiety in this respect.

3.2 Spatial resolution

OSMOND was installed on the CRISP reflectometer, positioned 2.2m from the CRISP sample position, see figure 9. The neutron beam enters the CRISP experimental blockhouse and is then collimated down through two sets of horizontal cadmium slits (S1 and S2, 2.59m apart), which define the beam at the sample position a further 0.36m downstream. The slits extend 50mm in the horizontal plane (hence OSMOND's 50mm drift depth) and the vertical slit width is computer controlled to an accuracy of the order of microns.

The data obtained from OSMOND can be interrogated in several different ways. When we are interested in variations with neutron wavelength (neutron energy) then we must use the ISIS DAE system as this time stamps the events over the 20000μs ISIS bunch length. If this is unimportant then the system can be run in a diagnostic mode were the encoded events can be observed along with the raw events. In this mode the data is summed over all time frames. Figure 10 shows the beam image obtained from OSMOND when both slits are set to 0.2mm, obtained in 100 seconds. The figure shows the DAE data and Gaussian fit to this data. A series of measurements were undertaken, where the slit settings were increased from 0.1mm to 0.75mm, for various settings of lower level discriminator setting (LLD). Fits to each data set yield a FWHM beam resolution which is shown for the whole series of measurements in figure 11. The FWHM obtained is lower with increasing LLD, as expected, and is sub mm for the smallest slit settings. The curves of figure 11 show a puzzling increase in the FWHM as the slits become very narrow. There is no obvious mechanism by which the detector could cause this and it may be due to a slit-generated halo of the beam becoming significant and wrapping into the detector response. If this contribution is ignored, a standard convolution fit to the highest slit width data, shown in figure 11, gives an improved resolution compared to that measured - 0.68mm compared to 0.72mm for an operating LLD of 0.6 and a slit width of 0.2mm. The fit also highlights a likely intrinsic detector FWHM of 0.59mm for a typical operating LLD of 0.6.

The linearity of the detector was investigated by illuminating OSMOND with a narrow beam (S1=S2=0.3mm) and by moving the detector mount vertically over 5mm in steps of 0.5mm. In this case the data was obtained from OSMOND using the DAE, and is summed over all time frames. If we fit Gaussian distributions to each of these data sets we obtain the data shown in figure 12 for the fit position (detector channel no.) and width of beam (sigma). The fit to the position data shown in figure 12 shows that the detector response is perfectly linear. The position resolution of the detector is geometrically defined and the spatial resolution is independent of position. Because of the "pointing" geometry a linear scan can only be done over a limited range before parallax effects appear.

The linear display of the tightly collimated beam profile in figure 10 does not reveal the existence of a low intensity halo around the basic Gaussian response curve. A logarithmic plot such as figure 13 reveals it very clearly. The main neutron beam image (around channel 548) sits on a secondary broad peak, of the order 350-450 channels wide which in turn is sat on a very low background of less than 1Hz count rate. This broad peak is clearly a beam halo induced by scattering. It should be stressed that several dead and malfunctioning channels have been linearly interpolated out in the figure. The integral counts in the halo represent a fraction of ~12% of the total. This halo is a feature of all position sensitive neutron detectors and results from the propensity of the neutrons to elastically scatter in the materials of the detector before being detected; in the case of OSMOND the main sources of scattering are the window and the displacer.

3.3 Counting rate performance

In order to investigate the counting rate characteristics of the OSMOND system, a series of measurements were made with the CRISP S1 and S2 slit separation increasing from 0.3mm up to a maximum of 8.0mm. Figure 13 shows the data obtained from the DAE (summed over all flight times) for the case of S1=S2=8.0mm and also for S1=S2=0.3mm. Both acquisitions were for 5000 time frames, which with a machine repetition rate of 40Hz is equivalent to 125 seconds. A dynamic counting range of five orders of magnitude is highlighted in the figure.

The global rate data for this series of measurements is summarised in figure 14, where the global raw data rate from the channel scalers is compared to the peak data rate measured from the DAE. A fit to the data in the figure shows an excellent fit to the deadtime formula, and gives us a measured deadtime of 505ns. The RPE has an intrinsic deadtime of 370ns, but this does not include any propagation delays in the system which is likely to be of the order of 40-50ns in total, giving a total deadtime of closer to 420ns, which is in reasonable agreement to the measured value.

This situation could be drastically improved if each individual detector channel had its own DAE channel. The maximum possible global counting rate (uniform irradiation) would then be similar to that obtained with the HOTWAXS detector [9], at approximately 500MHz with a single channel limit of 1-1.5MHz. This is currently not an

option, but it is thought that it may be possible to implement this in the next upgrade of the ISIS DAE system (DAE3) which is currently being developed.

3.4 Detector efficiency

A detection efficiency of >50% for 1Å neutrons was one of our requirements for OSMOND in order to make the most use of the neutrons produced from CRISP. The theoretical neutron detection efficiency for a 65mm gas depth of ^{3}He at a pressure of 3.6 bars is shown in figure 15 for the wavelength range of 1-5Å. In practice we will cut down on this theoretical maximum due to a combination of the need to discriminate against multiple hit events convoluted with the readout sampling pitch and diffusion in the gas. These have been investigated using the Monte Carlo simulation described in [8] with settings of 350keV for the LLD and a diffusion constant of 150$\mu m/\sqrt{cm}$. For the case of 3.6 bars of ^{3}He and 4.0 bars of CF_4 we obtain a value of 51.8% at 1Å compared to the theoretical value of 84.9%.

A cross-calibration of the detection efficiencies of OSMOND, a ZnS:Ag/^{6}LiF detector, and the CRISP beam monitors revealed that the experimental efficiency obtained at 1Å was 35.5%. The modelled efficiency (as a function of wavelength) shown in figure 15 (lower curve) which includes the readout efficiency and the transmission factor for 10mm of quartz [12] applied to the nominal absorption efficiency of 65mm of 3.6bars of ^{3}He (figure 15 upper curve) is seen to correspond reasonably well to the estimated efficiency values derived from comparison with the ZnS detector. The upstream and downstream monitors were used to normalise the two sets of data and the theoretical efficiency of the ZnS:Ag/^{6}LiF detector was used as the ultimate reference. The absorption in the 5mm aluminium window is estimated to be only 2% (at 1Å) and is neglected.

The detector efficiency is (inevitably) a function of the common threshold (LLD) set on the channel discriminators. Figure 16 shows the typical response of the output rate of the RPE as the LLD is varied. The LLD value is calibrated relative to the pulse height corresponding to the mean peak deposit of the 764keV detection reaction. As figure 16 shows the relative trigger efficiency declines little until the LLD reaches above a value of 0.6 which is the favoured operating point. The LLD at the time of the calibration of figure 15 is estimated to have lain in the upper region (between 0.8 and 0.9) so that the overall detection efficiency at an LLD of 0.6 is likely to be nearer to 45% at 1Å than the 35% that is measured.

Comparison of figures 11 and 16 show that there is a trade-off between spatial resolution and detection efficiency available from the LLD setting. A value of LLD=0.6 is taken as a good compromise (giving a sub mm FWHM spatial resolution and ~93% trigger efficiency); however, it is found that at LLD=0.9, ~98% of events trigger only one channel giving a notional resolution of ~0.35mm FWHM.

The gamma sensitivity of the detector to ^{60}Co gammas has not been measured, but should be a similar level to that obtained in the FastGas detector [3] around 1×10^{-5} for an LLD of 350keV (~0.45 on the current LLD scaling).

4. Application to Off Specular reflectometry

Neutron reflectometry is a technique employed for measuring the structure of thin films. The technique provides information over a wide variety of scientific and technological applications and involves shining a highly collimated beam of neutrons onto an extremely flat surface and measuring the intensity of reflected radiation as a function of angle or neutron wavelength. The shape of the reflectivity profile provides detailed information about the structure of the surface, including the thickness, density, and roughness of any thin films layered on the substrate. A super mirror was used to reflect the neutron beam, which is made of a multilayered stack of FeCoV/TiN [22]. An angular scan of the super mirror, from 0.35^{o} to 1.50^{o} in 0.05^{o} steps, was performed and a data set was obtained at each position. Figure 17 shows the data set obtained with the super mirror at an angle of 1.4^{o} for which the intensity is plotted on a log scale (again the dead and malfunctioning channels have been interpolated). A component of the beam impinging on the mirror is transmitted straight through the mirror, which is seen around channel 530. The high intensity feature around detector channel number 300 is the main reflected neutron beam, which is most intense after 17000μs. The feature seen beginning at detector channel number 375, at time 6650μs, is the most interesting. This is off-specular reflection from the super mirror which is known as Yoneda scattering, and is due to the surface roughness. Both the intense transmitted and the main reflected peaks show the detector response halos on the logarithmic display; the fact the bright features are 14000μs apart (i.e. several Å in wavelength), implies that the magnitude of the halo is independent of wavelength.

5. Conclusions

The OSMOND development programme has successfully produced a high counting rate detector with sub-mm position resolution capable of replacing the existing rate limited scintillator detector currently in use on the CRISP reflectometer for off specular reflectometry experiments. The count rate performance of the detector as installed for this test has been shown to be >5 times that of the current scintillator detector, whilst also offering good timing resolution and low gamma sensitivity at high neutron detection efficiencies in the 1-10Å wavelength range.

The detector is already fairly well optimised due to preliminary Monte Carlo modelling studies [8]. However figure 15 points towards the desirability of closing the gap between the measured detection efficiency and the intrinsic stopping power of the ^{3}He (increasing the partial pressure of which would result in almost negligible gain in efficiency). Two options present themselves: first (and simplest) the spare pressure capacity of the vessel (10 bars) could be utilised with a greater partial pressure of CF_4.

This would both reduce the range of the reaction products and reduce electron diffusion; second, the internal window structure could be modified to reduce the displacer thickness to 2-3mm while still collecting events from the gas space, thus increasing efficiency by a useful fraction while reducing the response halo effect.

The outstanding task remaining to realise the full potential of the detector is that of remediating the faulty channels seen in figure 5. That is in hand and it is hoped to approach the field uniformity of a few percent known to be possible with the technology. Fortunately in application to the field of reflectometry the presence of a few bad channels is not a serious problem.

With its current priority encoded readout, the rate performance of OSMOND is limited to a maximum rate of 1-1.5MHz. Whilst this may suffice for CRISP, for which further experimental testing will be required to determine, the ISIS second target station now has a further three reflectometer instruments (INTER, OFFSPEC and POLREF), where the neutron flux is a factor of 10 to 20 times greater than that currently obtained on CRISP. This situation could be remedied with next upgrade of the ISIS data acquisition system, DAE3 when full use could be made of the multi-scaler rate capacity of the detector.

Detectors of this type, offering a higher rate capability and improved position resolution, are expected to have a significant impact on the science programme for the reflectometers at ISIS in the near future.

This development has been funded via the facilities development board of the Science and Technology Facilities Council and by ISIS through the internal agreement between the ISIS and Technology departments.

References

1. A.Oed, Nucl. Instr. & Meth. A261(1988) 351
2. J.E.Bateman, G.E.Derbyshire, D.M.Duxbury, A.S.Marsh, N.J.Rhodes, E.M. Schooneveld, E.J.Spill and R.Stephenson, IEEE Trans. Nucl. Sci **52 (5)** (2005) 1693
3. J.E.Bateman, R.Dalgliesh, D.M.Duxbury, S.A.Holt, D.M^{c}Phail, A.S.Marsh, N.J.Rhodes, E.M.Schooneveld, E.J.Spill and R.Stephenson, Nucl. Instr. and Meth. **A616** (2010) 59
4. J.Penfold, R.C.Ward and W.G.Williams, J. Phys. E: Sci. Instrum. **20** (1987) 1411
5. J.Penfold, Physica B **173** (1991) 1
6. R.Bouclier, M.Capeans, G.Manzin, G.Million, L.Ropelewski, F.Sauli, L.I.Shekhtman, T.Temmel, G.Della Mea, G.Maggioni and V.Rigato, CERN Report, CERN-PPE/95-37
7. J.E.Bateman, J.F.Connolly, Yu.N.Pestov, L.I.Shekhtman, R.Mutikainen and I.Suni, Rutherford Appleton Laboratory Report, RAL-94-114
8. J.E.Bateman, D.M.Duxbury, N.J.Rhodes, E.M.Schooneveld, and R.Stephenson, RAL-TR-2006-005

9. J.E.Bateman, G.E.Derbyshire, G.Diakun, D.M.Duxbury, J.P.A.Fairclough, I.Harvey, W.I.Helsby, J.D.Lipp, A.S.Marsh, J.Salisbury, G.Sankar, E.J.Spill, R.Stephenson and N.J.Terrill, Nucl. Instr. and Meth. **A580** (2007) 1526
10. Swagelok, 29500 Solon Road, Solon, OH 44139 USA
11. Garlock (GB) Ltd, Premier Way, Lowfields Business Park, Elland, Wesy Yorkshire, UK, HX5 9HF
12. S.Holt, private communication
13. IMT, Greifensee, Switzerland
14. Schott Glass, Duryea, Pennsylvania, USA
15. JAE Europe, Coliseum Business Center, Riverside Way, Camberley, Surrey GU15 3YL U.K
16. Torrseal
17. Martech or Allectra
18. M.W.Johnson, S.P.Quinton, SNS data acquisition electronics (DAE), RAL-NDRP-8504
19. ATLAS Internal Note, INDET-NO-076 (1994)
20. J.E.Bateman, J.F.Connolly, G.E.Derbyshire, A.S.Marsh, R.Stephenson, R.C.Farrow, W.I.Helsby, B.R.Dobson, R.Mutikainen and I.Suni, RAL-TR-1998-073
21. J.E.Bateman, J.F.Connolly, G.E.Derbyshire, D.M.Duxbury, J.A.Mir, E.J.Spill, R.Stephenson, Nucl. Instr. and Meth. **A484** (2002) 384
22. SwissNeutronics AG, Bruehlstrasse 28, CH-5313, Klingnau, Switzerland

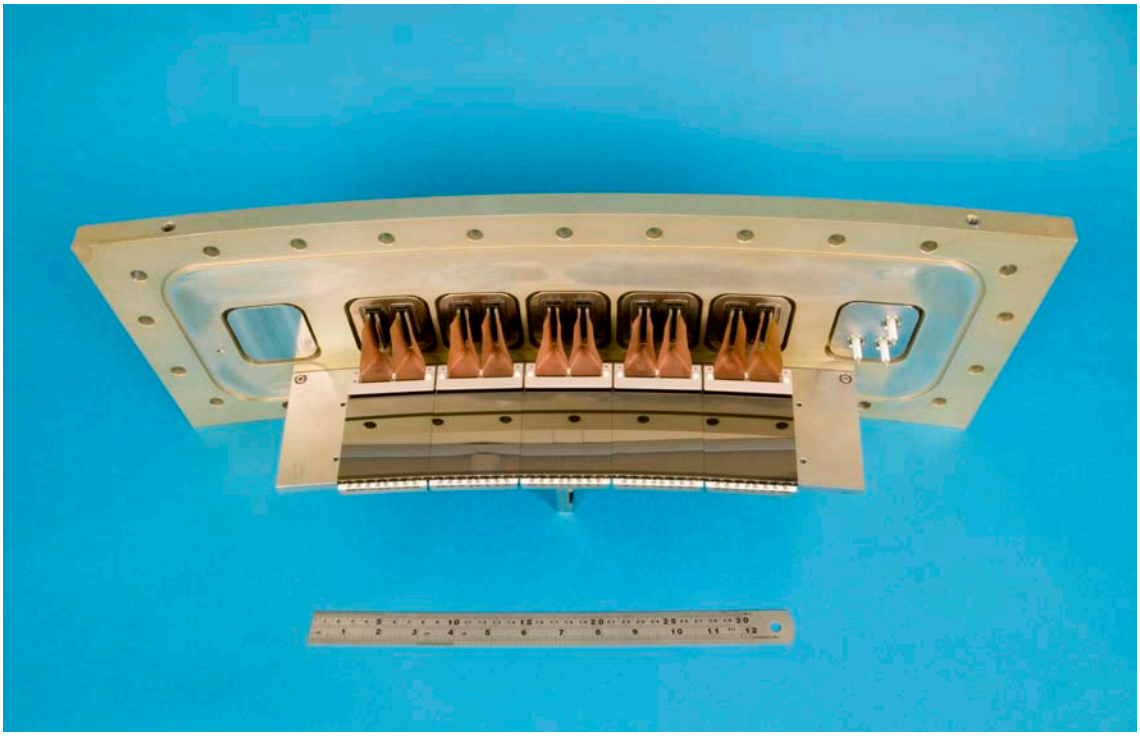

Figure 1: Partially assembled OSMOND detector showing the five MSGC modules

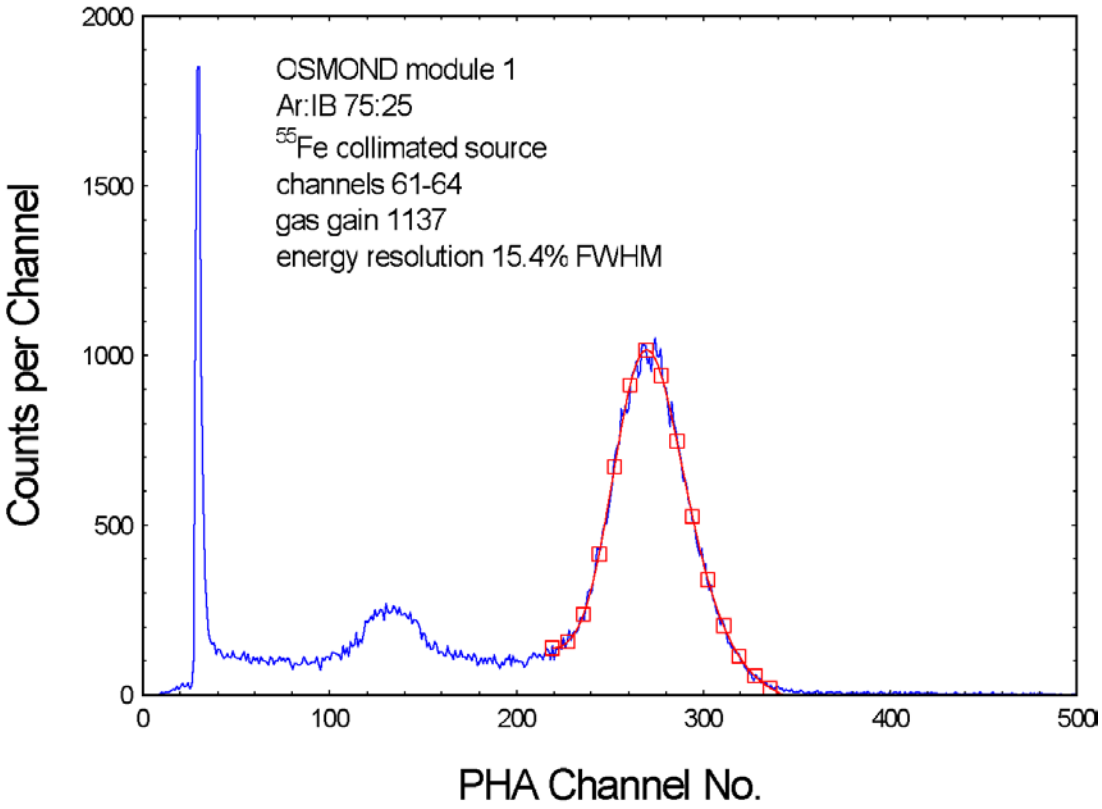

Figure 2: ^{55}Fe spectrum from sum of 4 consecutive channels

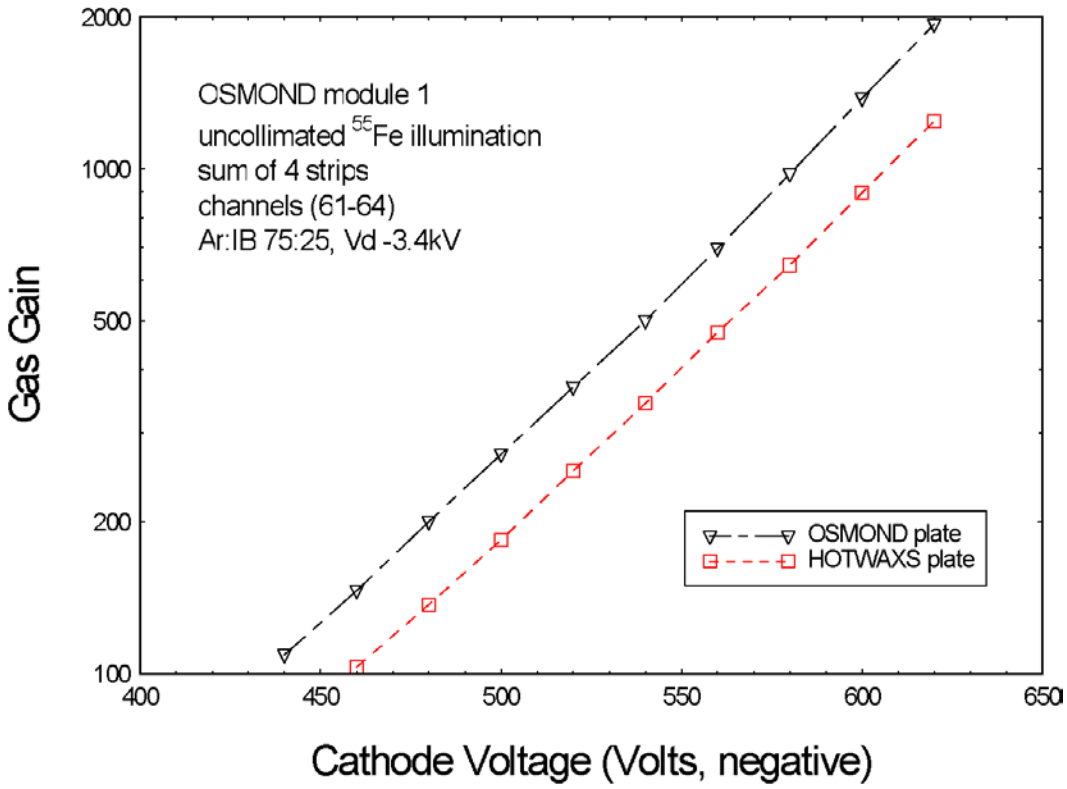

Figure 3: Gas Gain curves obtained with OSMOND module no.1

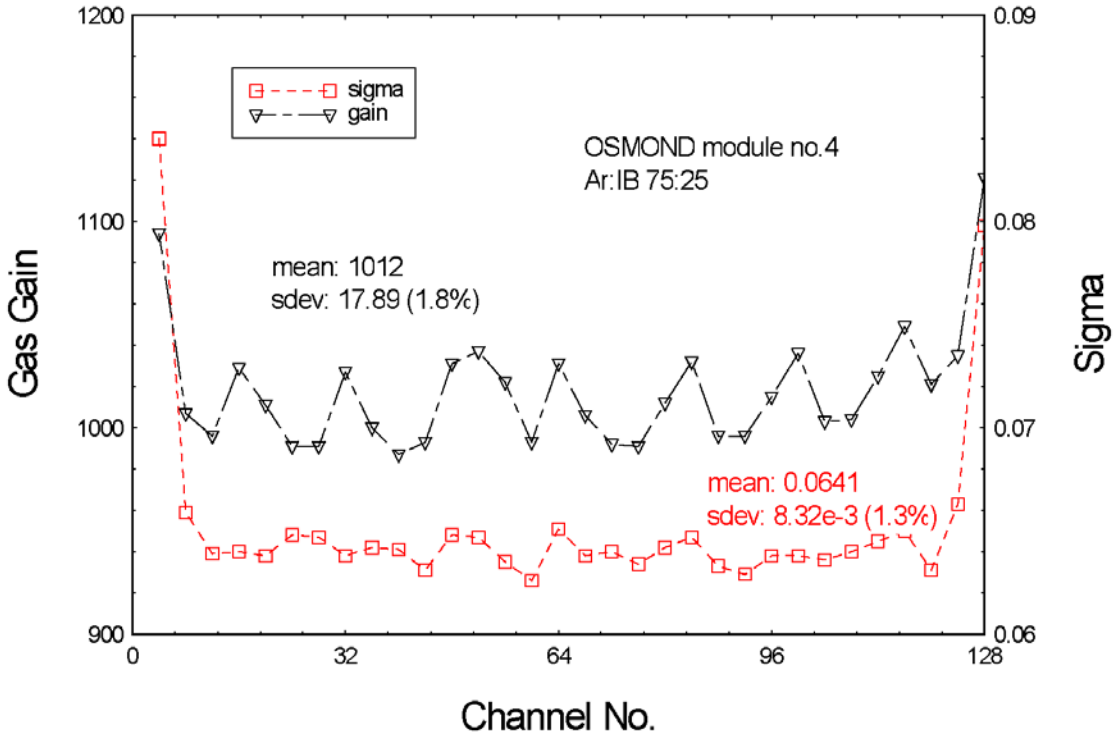

Figure 4: Variation of gas gain and pulse height resolution across module no.4

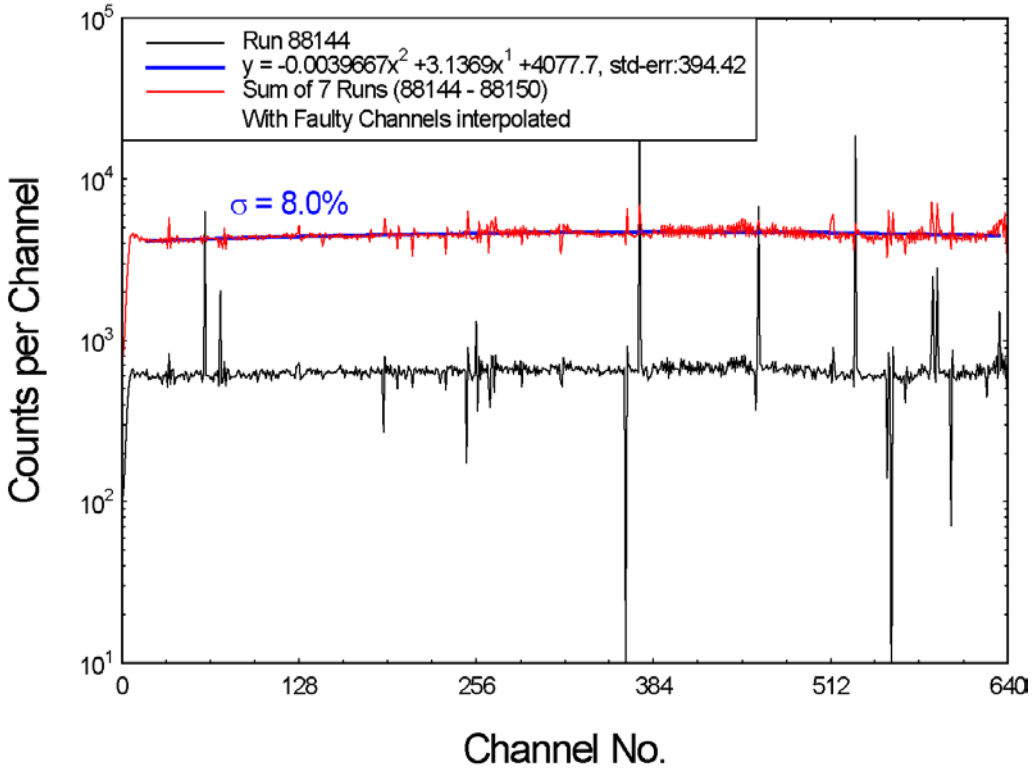

Figure 5: Detector flood response generated by the irradiation of a polyethylene block

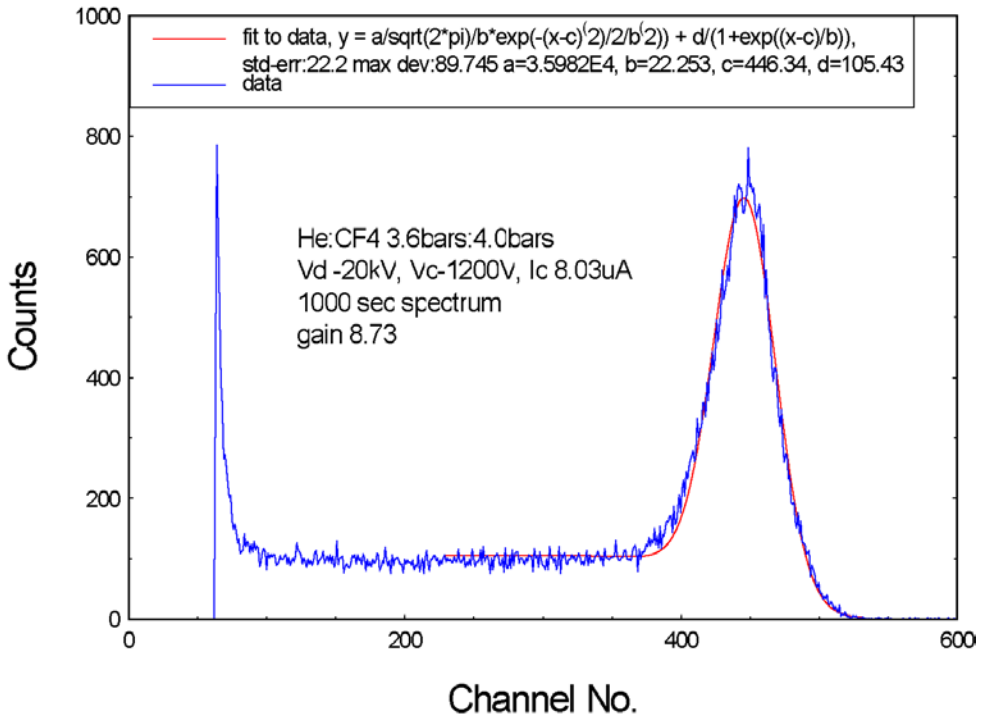

Figure 6: Pulse height distribution from the sum of 4 channels illuminated with a moderated ^{241}Am:Be source

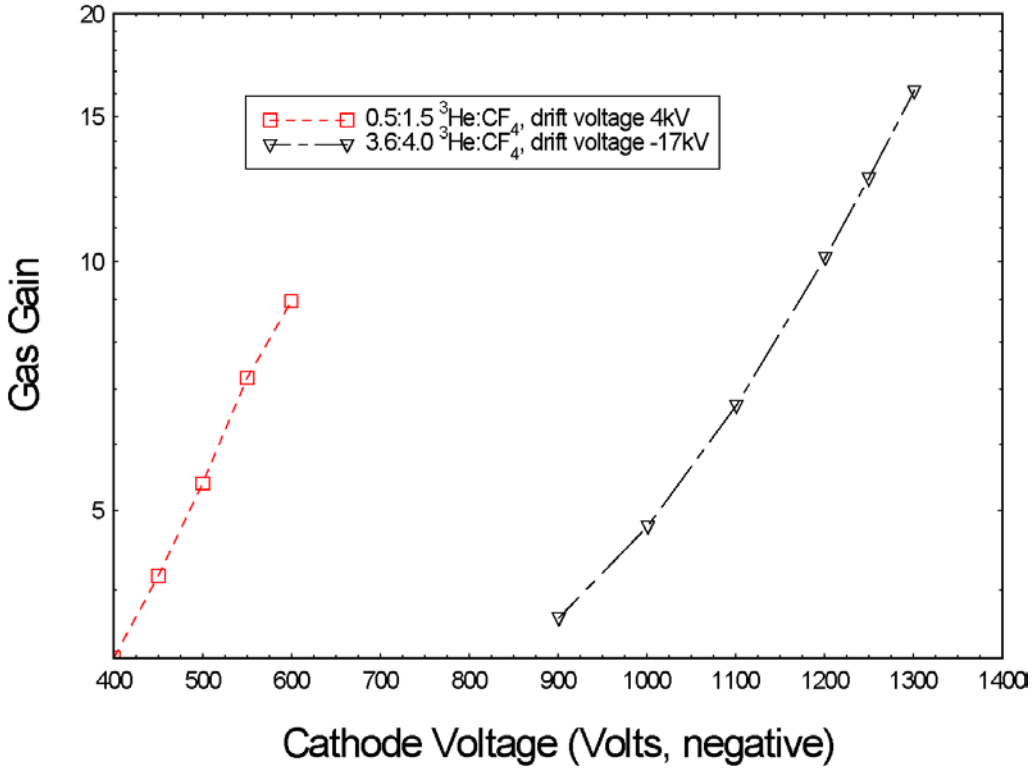

Figure 7: OSMOND gain curves in $^{3}He:CF_4$ gas mixtures

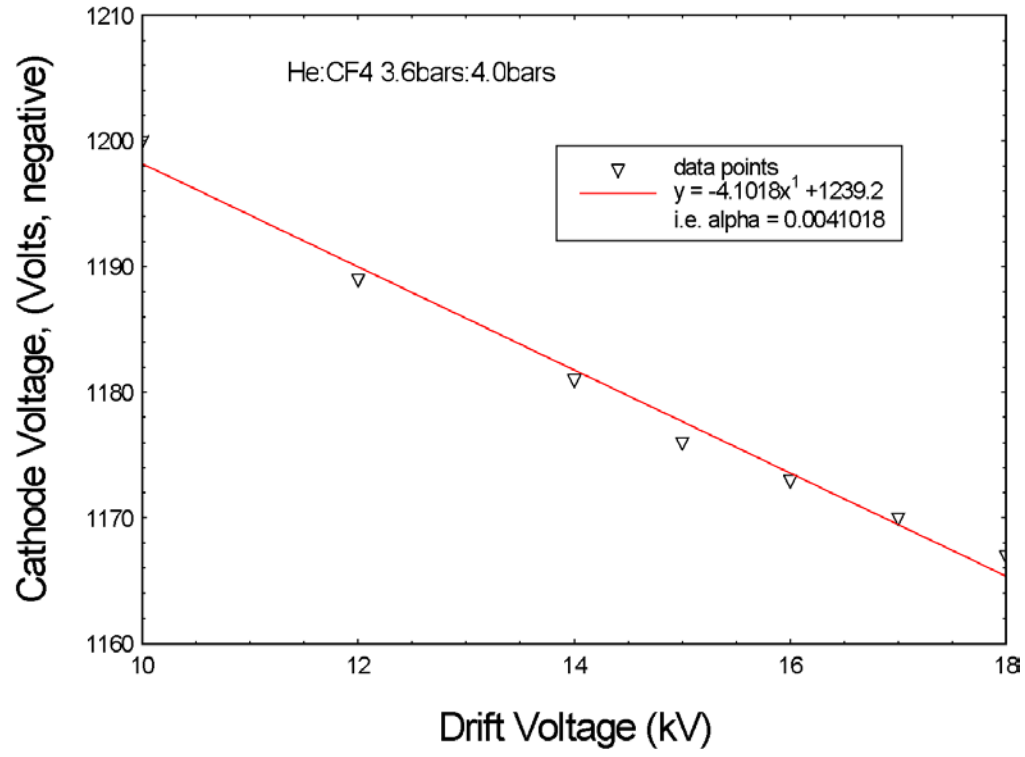

Figure 8: Plot of the cathode voltage versus the drift voltage for OSMOND

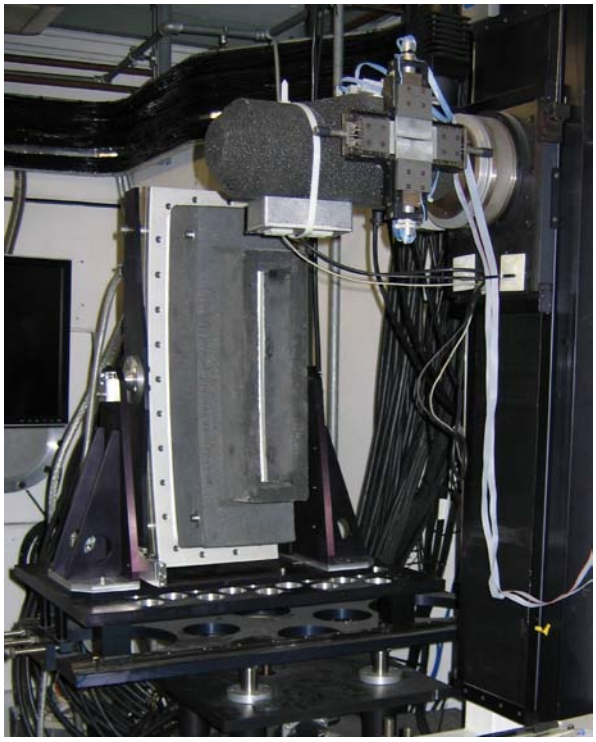

Figure 9: Photograph showing detector orientation on CRISP.

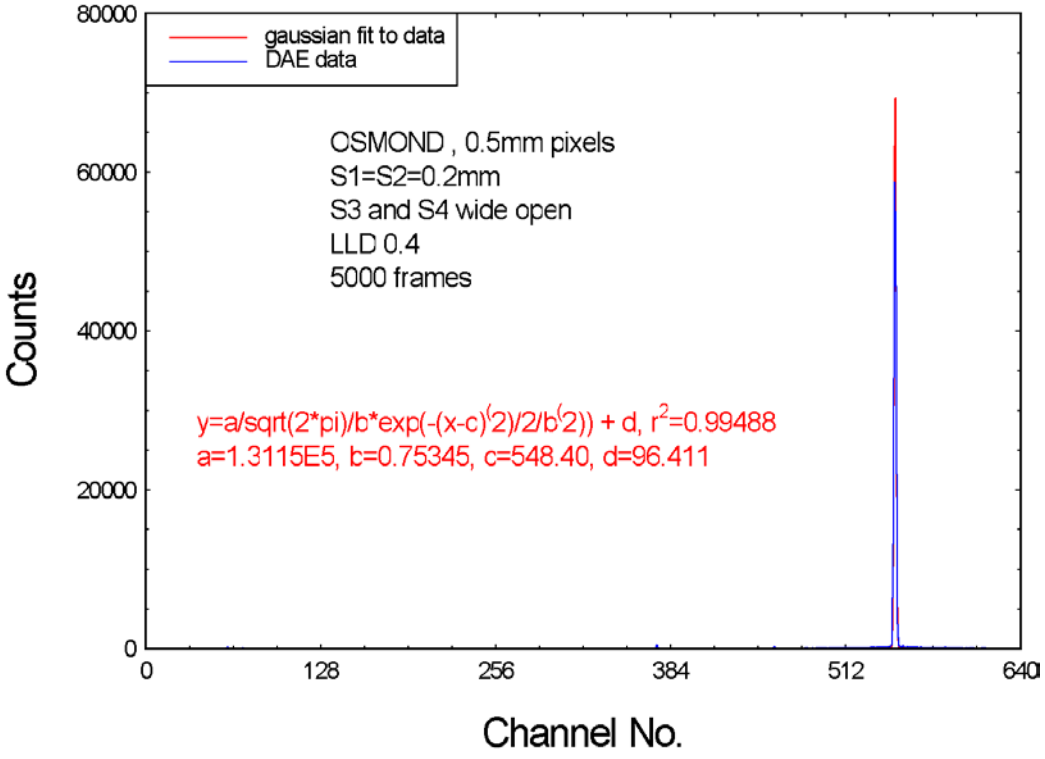

Figure 10: Data obtained from OSMOND with CRISP slits S1=S2=0.2mm wide

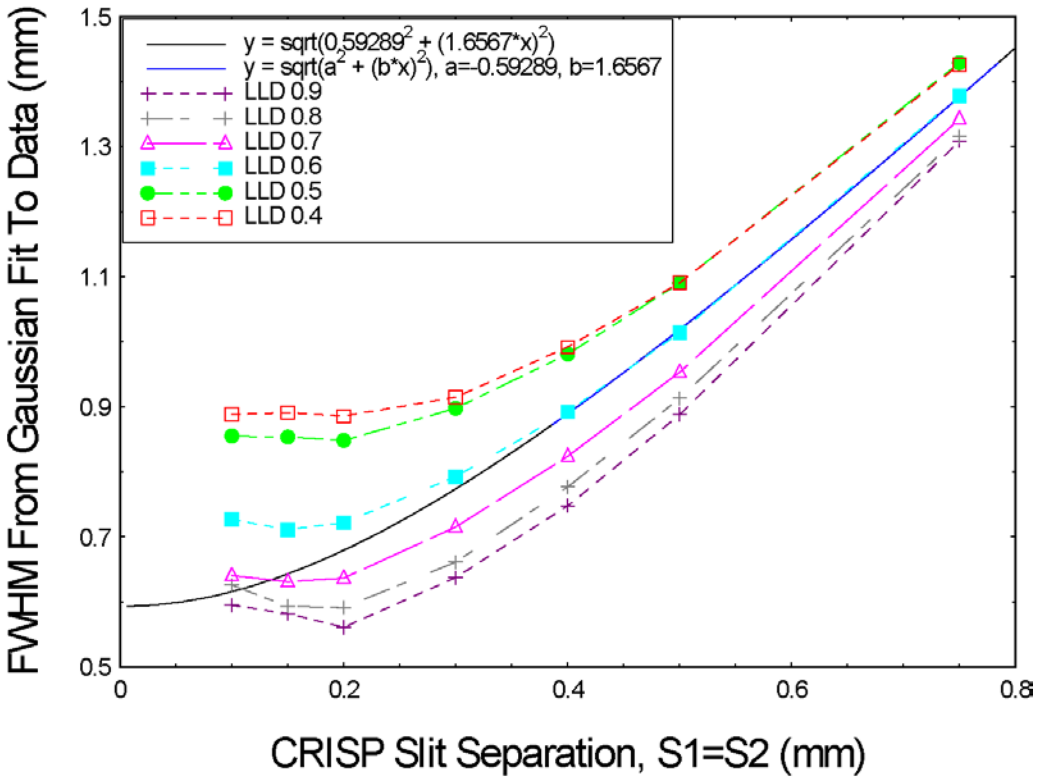

Figure 11: Variation of FWHM obtained from fit to slit data for various LLD settings

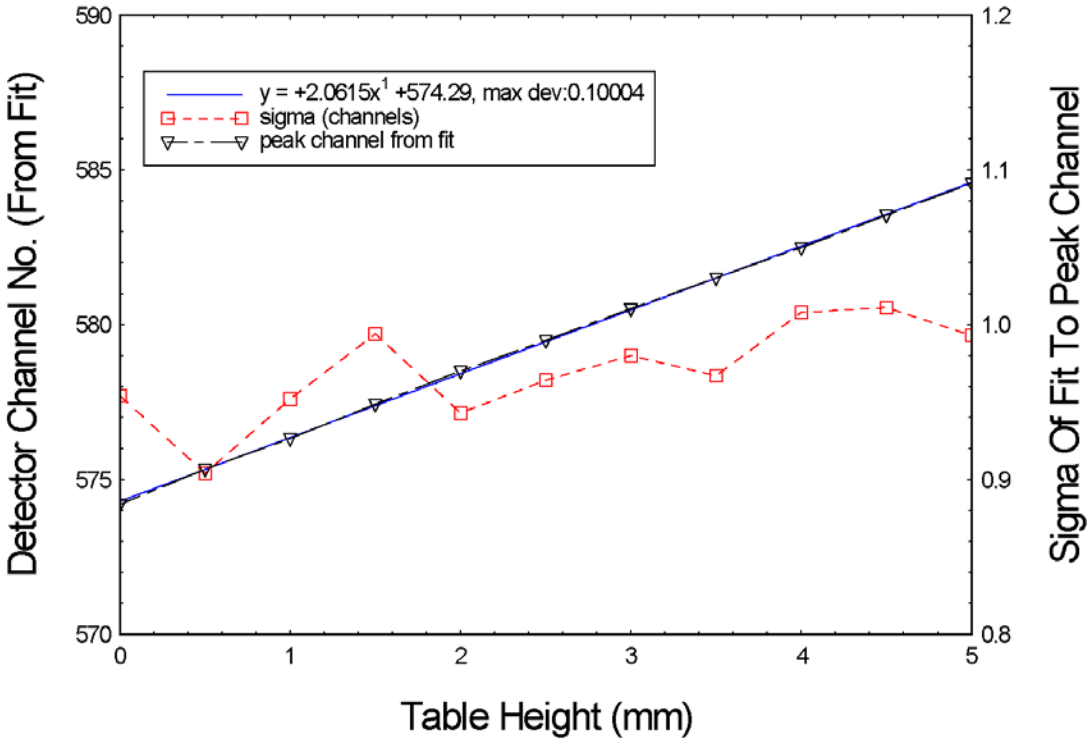

Figure 12: Channel number and sigma variation over 5mm detector mount scan

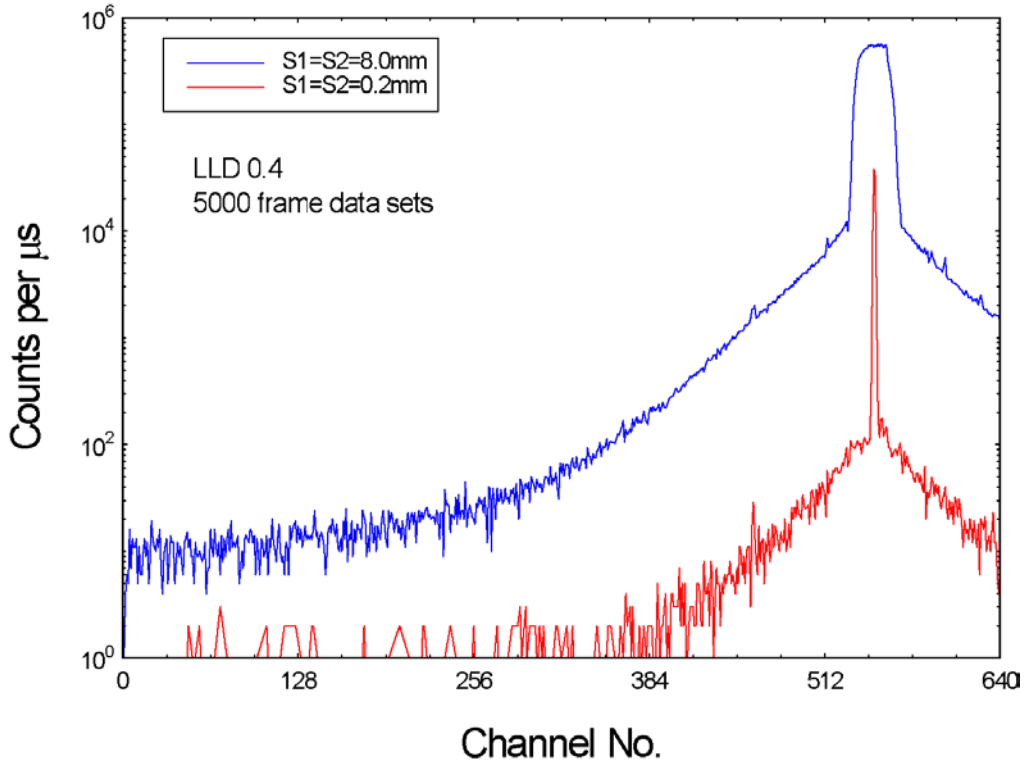

Figure 13: Beam response of OSMOND for S1=S2=0.2mm and S1=S2=8.0mm

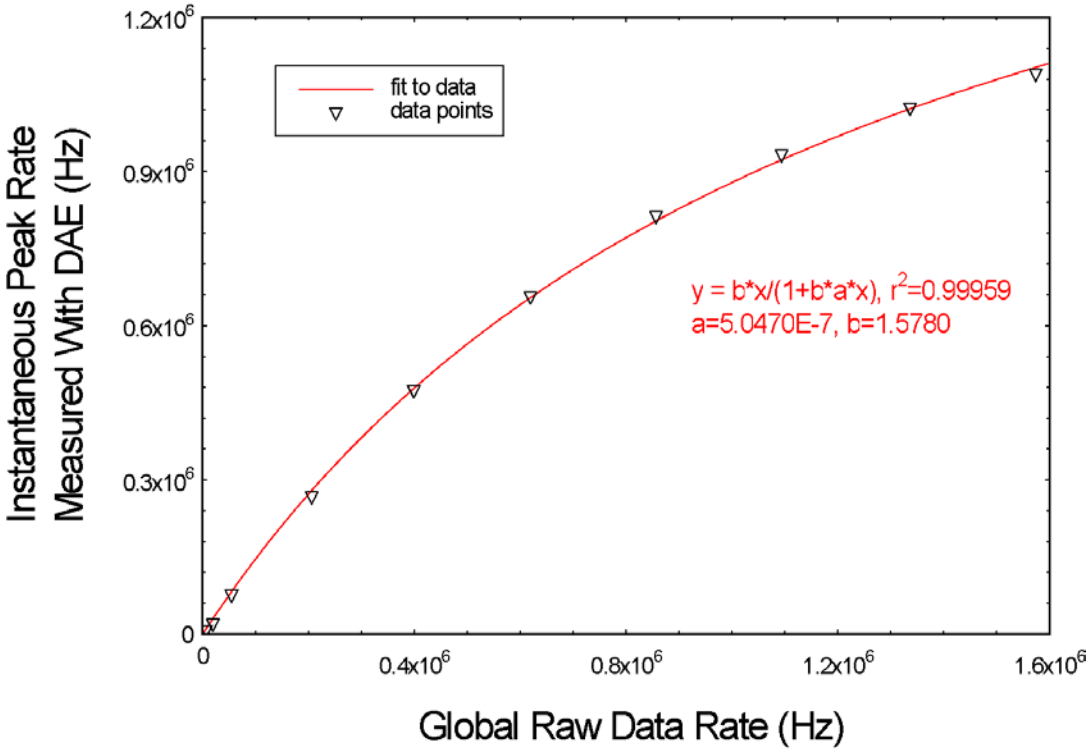

Figure 14: Instantaneous peak DAE rate versus raw data rate

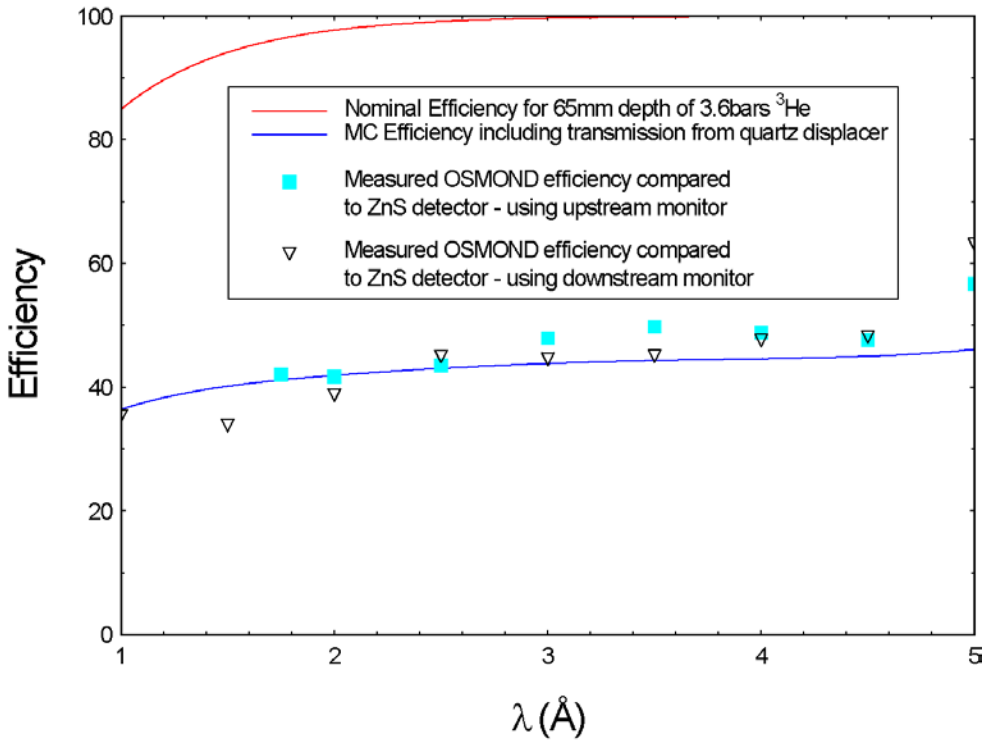

Figure 15: Relative efficiency of OSMOND as measured on CRISP

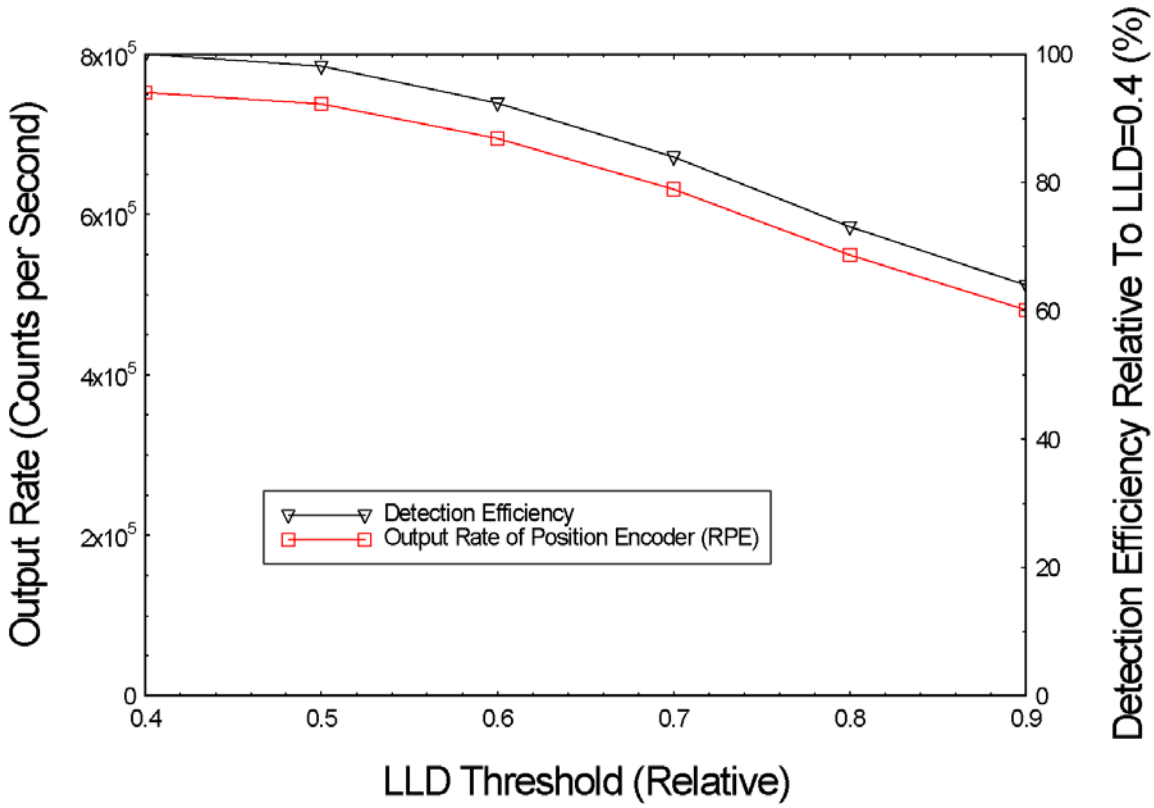

Figure 16: Output rate and trigger efficiency of the RPE readout system versus LLD

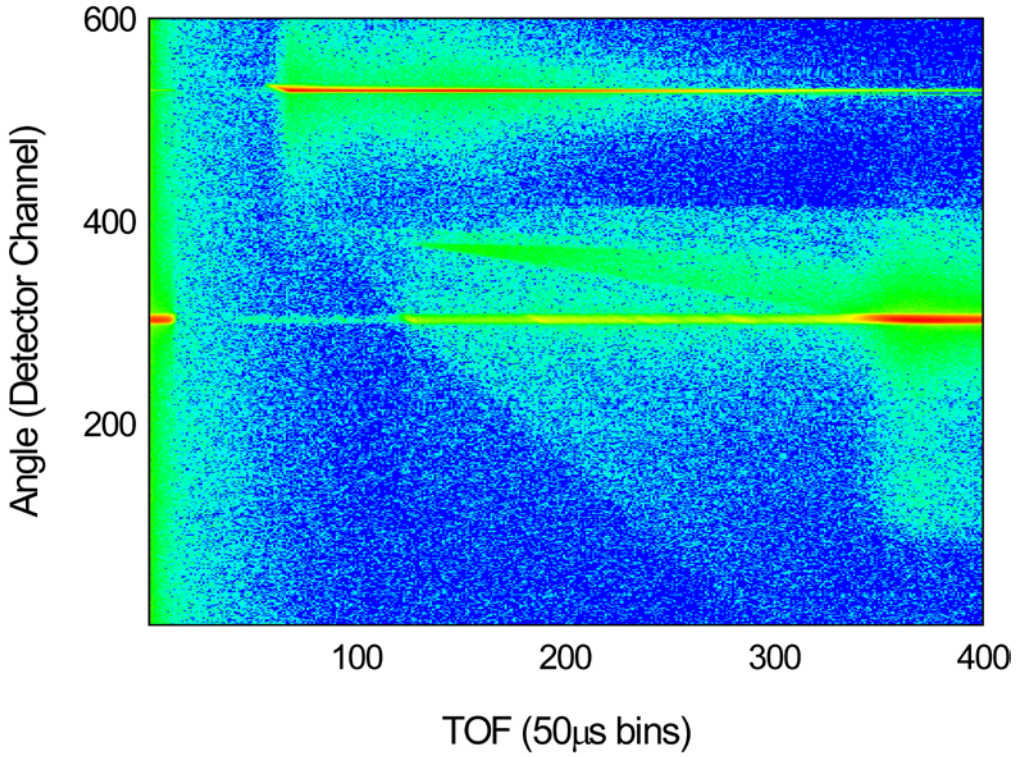

Figure 17: Data set for super mirror angle of 1.4^{o}